

DTIC FILE COPY

MTL TR 88-47

AD



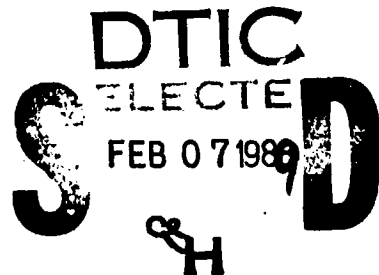
# WELDABILITY OF 2519-T87 ALUMINUM ALLOY

AD-A203 519

JACK H. DEVLETIAN, SANDRA M. DeVINCENT, and  
STEVEN A. GEDEON  
MATERIALS PRODUCIBILITY BRANCH

December 1988

Approved for public release; distribution unlimited.



**US ARMY**  
**LABORATORY COMMAND**  
MATERIALS TECHNOLOGY LABORATORY

**U.S. ARMY MATERIALS TECHNOLOGY LABORATORY**  
Watertown, Massachusetts 02172-0001

89 2 6 172

UNCLASSIFIED

SECURITY CLASSIFICATION OF THIS PAGE (When Data Entered)

REPORT DOCUMENTATION PAGE		READ INSTRUCTIONS BEFORE COMPLETING FORM
1. REPORT NUMBER MTL TR 88-47	2. GOVT ACCESSION NO.	3. RECIPIENT'S CATALOG NUMBER
4. TITLE (and Subtitle)  WELDABILITY OF 2519-T87 ALUMINUM ALLOY		5. TYPE OF REPORT & PERIOD COVERED Final Report
		6. PERFORMING ORG. REPORT NUMBER
7. AUTHOR(s) Jack H. Devletian, Sandra M. DeVincent, and Steven A. Gedeon		8. CONTRACT OR GRANT NUMBER(s)
9. PERFORMING ORGANIZATION NAME AND ADDRESS U.S. Army Materials Technology Laboratory Watertown, Massachusetts 02172-0001 ATTN: SLCMT-MEM		10. PROGRAM ELEMENT, PROJECT, TASK AREA & WORK UNIT NUMBERS D/A Project: 1L162105.AH84 AMCMS Code 612015.H84
11. CONTROLLING OFFICE NAME AND ADDRESS U.S. Army Laboratory Command 2800 Powder Mill Road Adelphi, Maryland 20783-1145		12. REPORT DATE December 1988
		13. NUMBER OF PAGES 28
14. MONITORING AGENCY NAME & ADDRESS (if different from Controlling Office)		15. SECURITY CLASS. (of this report)  Unclassified
		15a. DECLASSIFICATION/DOWNGRADING SCHEDULE
16. DISTRIBUTION STATEMENT (of this Report)  Approved for public release; distribution unlimited.		
17. DISTRIBUTION STATEMENT (of the abstract entered in Block 20, if different from Report)		
18. SUPPLEMENTARY NOTES  Condensed version of this report is published in the Webbing Journal, July, 1988		
19. KEY WORDS (Continue on reverse side if necessary and identify by block number) Weldability , Aluminum alloys , Mechanical properties , Armor . JES		
20. ABSTRACT (Continue on reverse side if necessary and identify by block number)  (SEE REVERSE SIDE)		

UNCLASSIFIED

SECURITY CLASSIFICATION OF THIS PAGE (When Data Entered)

Block No. 20

ABSTRACT

Test results show that 2519-T87 is weldable to itself and to 5083-H131. A wide variety of filler metals, weld parameters, and post-weld heat treatments were studied to determine the effect on weld mechanical properties, hot crack susceptibility, microstructure, and ballistic integrity. Previously reported 2519-T87 weldment ballistic failures have been discovered to be invalid. New ballistic weldments of 2519-T87 welded to itself were successfully qualified to the shock test in MIL-STD-1946.

*Key work →*

UNCLASSIFIED

SECURITY CLASSIFICATION OF THIS PAGE (When Data Entered)

# CONTENTS

	Page
SUMMARY .....	1
INTRODUCTION .....	1
FRACTURE ANALYSIS OF PREVIOUS BALLISTIC WELDMENTS .....	2
EXPERIMENTAL PROCEDURE .....	3
RESULTS .....	4
DISCUSSION	
Mechanical Properties .....	6
Fractography .....	7
Weld Heat Input .....	8
Shielding Gas Composition .....	8
Deposition Rate .....	9
Post-Weld Heat Treatment .....	9
Hardness .....	9
CONCLUSIONS .....	10
FOLLOW-ON RESEARCH .....	11
ACKNOWLEDGMENTS .....	11



Accession For	
NTIS GRA&I	<input checked="" type="checkbox"/>
DTIC TAB	<input type="checkbox"/>
Unannounced	<input type="checkbox"/>
Justification	
By	
Distribution/	
Availability Codes	
Dist. Special	
A-1	

## SUMMARY

In this continuing research program, the newly developed 2519-T87 aluminum alloy is evaluated as a possible replacement for 5083-H131 and 7039-T64 aluminum for armor plate applications on U.S. Army combat vehicles. The purpose of this portion of the investigation is to evaluate the weldability of thick-section butt joints of 2519-T87 welded to itself and to 5083-H131.

Full penetration, double-V groove welds were deposited on 19-mm (3/4") and 32-mm (1-1/4") thick plates of 2519-T87 and 5083-H131 by the gas metal arc welding (GMAW) process using: (a) two levels of heat input, (b) two shielding gases, and (c) four filler metal compositions. The weldability criteria were based on tensile properties, hardness, Charpy V-notch (CVN) impact toughness, fractography, microstructure, level of porosity, resistance to hot cracking (varestraint test), and deposition rate.

Fractographic analyses of broken transverse tensile specimens of welded 2519-T87 plate using all four types of aluminum filler metal revealed a characteristic or preferred crack path which was located entirely within the weld metal. The majority of these fractures exhibited a ductile dimpled appearance with microvoid coalescence beginning at particles of  $\text{CuAl}_2$ . The crack path in similar welds deposited on corner and butt joint specimens, subjected to ballistic shock testing in accordance with MIL-STD-1946, followed the fusion line and exhibited slight regions of brittle fracture surrounded by mostly ductile microvoid coalescence fracture.

Corner joints of 32-mm (1-1/4") 2519-T87 weldments were successfully qualified to the MIL-STD-1946 ballistic shock test. Previous ballistic shock test results of 2519-T87 weldments were found to be invalid due to the test velocity being too high.

The microstructure of weld metal deposited using both levels of heat input and various alloy filler metals exhibited typical dendritic structures where the dendrite core was aluminum solid solution and the interdendritic spaces were filled with the eutectic phase.

The mechanical properties of weldments were most significantly affected by the filler metal composition. Post-weld aging and reduced heat input (10 kJ/in.) slightly increased yield strength and hardness. The shielding gas composition of 25%Ar-75%He was found to increase deposition rate by 30% and reduce the tendency to form lack of fusion defects when compared to results found when using 100%Ar shielding gas. The filler metals having the highest deposition rates were those with the lowest electrical conductivity. The highest was 5356 followed by 4043, 2319, and 4145, respectively. Increasing the cooling rate by using thicker plates slightly increased weld metal yield strength in both the as-welded and post-weld aged conditions.

Good tensile strength values were found for welds made with 2319, 4043, and 4145 filler metal. This was true both when welding 2519-T87 to itself and to 5083-H131. Percent elongation values appeared to be low for these welds, but percent reduction of area values were higher (around 6 to 20%, depending on base and filler material). The low ductility may not necessarily be a problem, however, because the ballistic shock fracture surfaces appear to be mostly ductile rather than brittle.

Varestraint tests show that both 4043 and 4145 are resistant to hot cracking. The 2319 can be made to exhibit cracks under extreme restraint conditions, but is probably acceptable for most production applications. Welds using 5356 filler metal were extremely hot crack susceptible and usually cracked in the root pass welds of 2529 to 5083.

It is anticipated that the results of this study will make the fabrication of 2519-T87 a viable option for Army applications. The 2519-T87 exhibits a superior combination of ballistic, stress corrosion cracking, and tensile performances compared to other aluminum alloys.

## INTRODUCTION

Two aluminum alloys, 7039-T64 and 5083-H131, have accounted for the majority of armor and structural applications for U.S. Army light combat vehicles to date. Recently, Alcoa introduced a new precipitation hardening alloy designated 2519-T87 aluminum (conforming to MIL-A-46192), which combines the good strength and ballistic performance of the 7039-T64 aluminum alloy with the good stress corrosion cracking resistance of the 5083-H131 aluminum alloy.

The 2519-T87 aluminum alloy is being evaluated as a potential alternative to these alloys to provide adequate armor protection, stress corrosion resistance, and weldability. In addition, the use of a single alloy to replace two alloys will help solve production problems associated with tracking two different alloys throughout a plant.

All the 2519 material studied in this report was in the T87 temper condition and the 5083 was all in the H131 temper condition. Henceforth, the 2519-T87 will be referred to simply as 2519 and the 5083-H131 as 5083.

Although initial studies on the weldability of 2519 aluminum (formerly Alcoa's CV34) have been reported,<sup>1-3</sup> additional research was needed to broaden the existing data base compiled on this new alloy for future Army utilization. If the 2519 alloy is selected as a primary aluminum armor component on combat vehicles, weldability data for 2519 will become essential to designers and structural engineers. In addition, dissimilar metal joints between 2519 and 5083 may be structurally critical. Also, the various appurtenances welded to the primary armor are currently fabricated from 5083 aluminum.

The purpose of this investigation was to evaluate the weldability of 2519 welded to itself and to 5083 using the GMAW process. The weldability assessment was based on the level of porosity, resistance to hot cracking (via the vareststraint test), transverse-to-weld tensile properties, hardness, CVN impact toughness, microstructure, and deposition rate. The principle welding variables in this investigation included: shielding gas composition, filler metal composition, level of heat input, plate thickness, and post-weld heat treatment.

The results of this study will provide a preliminary screening of welding variables to minimize the number of weldments needed for costly ballistic tests per MIL-STD-1946. In addition, the larger data base for the 2519 aluminum alloy may permit a more cost-effective utilization of this alloy as a potential replacement for other lightweight materials on a variety of combat vehicles and aircraft.

### FRACTURE ANALYSIS OF PREVIOUS BALLISTIC WELDMENTS

In a previous report on this program,<sup>1</sup> a series of eight ballistic weldments were tested in accordance with the shock test in MIL-STD-1946. Four of these weldments were of 2519 welded to itself with 2319 filler metal and weld parameters very similar to those of Weld #4 in Table 1.

Table 1. WELDING CONDITIONS USED FOR EACH EXPERIMENTAL WELD

Weld No.	Schedule	Gas Shielding	Thickness of Plate mm (in.)	Types of Alloys Welded	Filler Metal
1	B	25Ar-75He	19 (3/4)	2519/2519	2319
2	A	25Ar-75He	↓	2519/2519	↓
3	A	25Ar-75He	↓	5083/2519	↓
4	A	100Ar	↓	2519/2519	↓
5	B	25Ar-75He	↓	5083/2519	↓
6	A	↓	↓	↓	5356
7	B	↓	↓	↓	4043
8	A	↓	↓	↓	4043
9	B	↓	↓	↓	4145
10	A	↓	↓	↓	4145
11	B	↓	↓	↓	5356
12	A	↓	↓	2519/2519	4043
13	A	↓	32 (1-1/4)	↓	2319
14	A	↓	19 (3/4)	↓	4145
15	A	↓	32 (1-1/4)	↓	4145
16	A	↓	32 (1-1/4)	↓	4043
17	A	100Ar	32 (1-1/4)	↓	2319

1. WOLFE, T.D., and GEDEON, S.A. *Weldability of 2219-T851 and 2519-T87 Aluminum Armor Alloys for use in Army Vehicle Systems*. U.S. Army Materials Technology Laboratory TR 87-28, June 1987.
2. LUCIA, E., and ANCTIL, A. *Laminate Armor for Light Combat Vehicles (U)*. U.S. Army Materials Technology Laboratory TR 86-14, April 1986, p. 185-196.
3. MARTUKANTZ, R.P. *Weldability of Ballistic Alloys CW33 and CW34 Weldments*. Alcoa Report PREN 52-83-31, 1983.

Since that report,<sup>1</sup> it was found that all four of the 2519 tests were invalid. All four tests, which were previously reported as failures, were actually fired at too high of a test velocity,<sup>4</sup> and thus must be discounted.

Three new weldments were made with the corner joints geometries shown in Figure 1 and the weld procedures and conditions listed for Weld #4 in Table 1. All three of these weldments were properly impacted twice in accordance with the ballistic shock test in MIL-STD-1946. Only weld joint C showed any signs of cracking. Weld C had cracking in excess of 12" and was the only failure.

Most importantly, Weld C was expected to fail because of its poor joint design. This provided additional evidence that MIL-STD-1946 can distinguish between good (A, B) and bad (C) welds. This was the first ballistic qualification of the weldability of 2519 aluminum.

Ballistic shock test specimens which exhibited weld fractures (from the first series of tests<sup>1</sup>) were examined optically and with a scanning electron microscope (SEM). Fractographic and metallographic analyses indicated that the fractures tended to propagate parallel, and very close, to the weld fusion line as evidenced by Figure 2. Despite the shock rate of loading, the fractures were essentially ductile as illustrated in Figure 3. The major mode of fracture was microvoid coalescence initiating primarily at CuAl<sub>2</sub> precipitates. A small portion of the fracture surface, near the fusion line, appeared to be brittle surrounded by patches of ductile fracture, as shown in Figure 4.

Based on the observation of a mostly ductile failure mechanism, it was anticipated that the ballistic shock resistance of 2519 weldments could be increased by (1) increasing the strength of the weld metal (through selection of filler metal type and post-weld heat treatment) and (2) reducing the amount of large crack-sensitive second phase precipitates between dendrites. Thus, in this investigation, reduced heat input welds and higher cooling rates were examined to determine the advantage of refined primary dendrite arm spacing (DAS) combined with smaller second phase precipitates. Based on the observation of small patches of apparently brittle fracture along the fusion line, temper beads were studied to understand and hopefully eliminate the possibility of a brittle fusion line region.

## EXPERIMENTAL PROCEDURE

The materials used in this investigation included: 19-mm (3/4") and 32-mm (1-1/4") thick plates of 2519 and 5083 aluminum alloys. These plates were machined into approximately 300-mm x 150-mm (12" x 6") sections. The double-V groove joint shown in Figure 5 was machined along one of the 300-mm (12") edges of each section in order to provide weldments for mechanical property evaluations. Chemical compositions of plate and filler materials are given in Tables 2 and 3.

Table 2. CHEMICAL ANALYSIS OF ALUMINUM ALLOYS

	Weight Percent										
	Cr	Cu	Fe	Mg	Mn	Ni	Si	Ti	V	Zn	Zr
2519-T87	—	5.60	0.15	0.19	0.28	0.007	0.06	0.06	0.05	0.07	0.1900
5083-H131	0.08	0.06	0.29	4.50	0.64	0.004	0.09	0.02	0.03	0.03	—
7039-T64	0.19	0.05	0.20	2.87	0.24	0.240	0.10	0.02	0.01	4.25	0.006

Table 3. CHEMICAL COMPOSITIONS OF ALUMINUM FILLER METALS

	Weight Percent											
	Be	Cr	Cu	Fe	Mg	Mn	Ni	Si	Ti	V	Zn	Zr
2319	0.0008*	—	6.3	0.30*	0.02*	0.3	—	0.20*	0.15	0.10	0.10*	0.18
4043	—	0.10	0.5-1.3	1.0	0.6-1.3	—	0.5-1.3	11-13.5	—	—	0.25	—
4145	—	0.15	3.3-4.7	0.8	0.15	0.15	—	9.3-10.7	—	—	0.20	—
5356	—	0.05-0.2	0.10	0.40	4.5-5.5	0.05-0.2	—	0.25	0.05-0.2	—	0.10	—

\*Maximum content

4. VAN CANEGHAN, R.J. *Re-test of Armor for Methodology and Specification Development (Ballistic Tests of 2519 Alloy Aluminum Armor and 2219 Alloy Aluminum Armor Plate)*. U.S. Army Combat System Test Activity Firing Record No. Ar-48902, TECOM Project No. 1-EG-965-000-476, 1987.

GMAW was performed using 1.6-mm (1/16") diameter filler metals of: 2319, 4043, 4145, and 5356 designations. Two levels of heat input were used: 994 J/mm (25.3 kJ/in.) and 394 J/mm (10 kJ/in.), designated Schedule A and B, respectively. In addition to pure argon shielding gas, a mixture of 25Ar-75He was evaluated primarily to provide penetration capability and weld bead shape suitable for GMAW heavy section aluminum plates. Welding parameters for both levels of heat input are given in Table 4.

Table 4. WELDING PARAMETERS FOR NORMAL HEAT INPUT (SCHEDULE A) AND LOW HEAT INPUT (SCHEDULE B) WELDS DEPOSITED BY GMAW

	Heat Input Level	
	Schedule A*	Schedule B
Current	265 A	200 A
Voltage	28 V	25 V
Travel Speed	0.67 mm/s (17 ipm)	1.2 mm/s (30 ipm)
Workpiece Position	Flat	Flat
Torch Inclination Angle	6	6
Preheat and Postheat	None	None
Interpass Temperature	150 Maximum	150 Maximum
Gas Flow Rate	80 CFH	80 CFH
Electrode Size	1.2 mm (1/16")	1.2 mm (1/16")
Cleaning Procedure	acetone scrub followed by stainless steel wire brush prior to first pass and wire brush for subsequent passes	
Backchipping	root pass only	

\*Two root passes were deposited with the low heat input parameters to avoid burnthrough

Table 1 summarizes the test matrix of welding conditions studied. The root pass was backchipped to ensure full penetration. The weld area was cooled to room temperature, washed with acetone, and stainless steel wire brushed between each pass. Each weld joint was radiographed to ensure that mechanical property specimens were free from defects. Welds were then saw cut into blanks for subsequent machining of tensile, CVN toughness, hardness, and metallographic specimens.

Several welded specimens were heat treated prior to testing. Post-weld heat treatments included: (1) aging at 204°C (400°F) for various times and (2) solution heat treating to 535°C (995°F), ice water quenching, and subsequent aging at 204°C (400°F). All heat treatments were conducted in furnaces with an air atmosphere.

Mechanical testing included uniaxial tensile, CVN impact toughness, and hardness tests. Standard round tensile bars having a 12.8-mm (0.505") diameter and a 50.8-mm (2") gage length were machined in accordance with MTL SP 77-10 Type T(R)-1. Specimens were tested at a crosshead speed of 1.27 mm/min (0.05 in/min). All tensile testing was performed at room temperature. CVN impact toughness specimens were machined to MTL SP 77-10, specimen CV-2, with the notch located in the center of the weld. Testing was performed in accordance with AWS Standard B4.0 at room temperature. Both Rockwell B and Knoop microhardness tests were used to measure the hardness characteristics of each weld metal, heat affected zone (HAZ), and base metal.

Metallographic specimens were prepared transverse to the weld in order to examine the weld metal, HAZ, and base metal. Weld joints were polished and etched with Keller's solution.

Varestraint tests were performed on the 2519 plates using GMAW with various filler metals to measure resistance to hot cracking. Crack length measurements were recorded after testing 12.5-mm (1/2") thick plate at the 4% augmented strain level in accordance with AWS standard B4.0. The varestraint specimens were machined so that after GMA welding, the top of the bead was flush with the upper surface of the specimen. This was done to ensure that the imposed strain equaled 4%.

## RESULTS

Four filler metals were used to weld 2519 to itself and to 5083: 2319, 4043, 4145, and 5356. A separate bar graph is shown for each mechanical property determination. Figure 6 shows the ultimate tensile strength (UTS) as a function of filler metal, heat input, shielding gas, and aging treatment. The first bar for each of the five welds indicates the UTS in

the as-welded condition, and the second bar shows the effect of post-weld aging at 204°C (400°F) for 1 hour. Weld #1 (the second set of bars in Figure 6) shows the effect of reduced heat input. Weld #4 (the third set of bars in Figure 6) shows the effect of using pure argon shielding gas rather than 25Ar-75He. Welds #12 and #14 (the fourth and fifth sets) show the effect of using 4043 and 4145 filler metal.

Similarly, Figures 7 through 9 display the resulting yield strength, percent reduction of area, and percent elongation for the same series of welds. No mechanical properties are shown for 2519 welded to itself with 5356 filler due to extensive hot cracking.

Figures 10 through 13 present the mechanical properties as a function of the same weld variations for the dissimilar base metal combination of 2519 welded to 5083.

Charpy V-notch results are shown in Figure 14 for 2519 welded to itself. Figure 15 presents the CVN values of 2519 welded to 5083. Unfortunately, a number of the CVN specimens had objectionable defects, and not all filler metal/base metal combinations were tested. However, it was determined that the CVN value for the unwelded 2519 base metal (5.9 ft-lb) is less than the CVN value of the 2319 and 4043 filler metals. The CVN toughness of the 5083 base metal was found to be 10.0 ft-lb.

The resistance to hot cracking was determined for both the filler metal and shielding gas composition. The 2319, 4043, and 4145 welds exhibited X-ray quality (per AWS Standard D1.2) and metallographically sound deposits on 2519 plates. The 5356 filler metal, however, developed severe hot cracking in the root passes of 2519 welded to itself and to 5083.

In order to determine the ranking of resistance to hot cracking for the 2319, 4043, and 4145 filler metals, the restraint test was performed using GMAW at an augmented strain level of 4%. These results are indicated in Table 5. As shown, 2319 is the most crack susceptible followed by 4145 and 4043. The 5356 filler metal was not tested due to severe hot cracking of root pass weldments of 2519 to 5083.

Table 5. VARESTRAINT RESULTS FOR 2519-T87 WELDMENTS

Filler Wire	Sample No.	Max. Crack Length (in.)	Total Crack No	No. of Cracks (Length > 0.1 in.)	Total Crack Length (in.)
Thickness of Base Metal, in.: 0.5 Diameter of Filler Metals, in.: 1/16 Welding Current, amps: 110 Welding Voltage, volts: 22 Augmented Longitudinal Strain, %: 4					
2319	1	0.144	21	8	1.82
	2	0.164	14	9	1.49
	3	0.152	20	7	1.59
	Average	0.153	18	8	1.63
4043	1	0.148	10	3	0.80
	2	0.223	8	2	0.73
	3	0.251	3	2	0.36
	Average	0.174	7	2	0.62
4145A	1	0.106	5	2	0.38
	2	0.121	6	2	0.43
	3	0.120	6	2	0.44
	Average	0.116	6	2	0.41
4145B	1	0.045	3	0	0.12
	2	0.112	5	1	0.29
	3	0.063	9	0	0.39
	Average	0.073	6	0	0.27

The 2519 was welded using two plate thicknesses, 19-mm (3/4") and 32-mm (1-1/4"), in order to examine the effects of cooling rate on weld properties. The thicker plate provided a greater heat sink and faster cooling rate per pass. Also, since about 20 passes were needed to weld the 32-mm (1-1/4") thick plate, a high percentage of filler metal was present in these welds. The resulting mechanical properties of these thicker base plates are shown in Table 6. As indicated, the slight increase in cooling rate has little effect on the mechanical properties.

Table 6. MECHANICAL PROPERTIES OF 19-MM (3/4") AND 32-MM (1-1/4") SIMILAR 2519-T87 TO 2519-T16/ WELDMENTS

Weld No.	Filler Metal	Shielding Gas	Plate Thickness (mm)	UTS (ksi)	2% YS (ksi)	RA (%)	ELon. (%)
2	2319	25Ar-75He	19	43.2	28.5	21.8	5.0
13	2319	25Ar-75He	32	44.8	30.2	17.9	3.8
8	4043	25Ar-75He	19	39.8	27.7	8.8	3.0
16	4043	25Ar-75He	32	38.8	28.1	19.9	3.5
4	2319	100Ar	19	43.4	27.3	17.3	3.8
17	2319	100Ar	32	45.3	32.1	11.5	2.9

Figures 16a, 16b, and 16c show Knoop microhardness traces of the weld fusion zone, HAZ, and base metal for bead-on-plate welds made with 2319, 4043, and 4145 on 2519. All three welds were made with the same parameters and conform to Welds #2, #12, and #14. Figures 17a, b, and c show microhardness readings on dissimilar root pass welds of 2519 to 5083 using 2319, 4043, and 4145 filler metals.

The effect of multiple pass welding is demonstrated in Figure 18. Here, a distinct increase in hardness is found in the fine equiaxed structure developed at the partially melted zone of adjacent beads. In order to understand this effect in a controlled experiment, a test resembling the "bead temper test" was performed. The effect on hardness of a second bead placed on top of the first bead is shown in Figures 19a, 19b, and 19c. In order to increase the strength of the weld metal, post-weld heat treatments were studied.

Figure 20 shows the hardness of the 2519 as a function of aging time at room temperature and at 400°F. As indicated, 2519 naturally ages at room temperature, but artificial aging does increase the hardness somewhat.

The choice of filler material and shielding gas composition affected the deposition rate. In order to quantify this effect, the voltage, electrode extension, and travel speed were held constant while the wire feed rate was adjusted to maintain a constant current. These results are presented in Table 7.

Table 7. WIRE FEED RATE NEEDED TO MAINTAIN CONSTANT WELDING PARAMETERS

				Voltage, volts:	26
				Travel Speed, ipm:	17
				Electrode Extension, in.:	3/4
				Current, amps:	265
Weld No.	Base Plates	Filler Metal	Shielding Gas	Wire Feed Rate	
				mm/s	(ipm)
4	2519/2519	2319	100Ar	102	(241)
2	2519/2519	2319	25Ar-75He	158	(374)
12	2519/2519	4043	25Ar-75He	165	(390)
14	2519/2519	4145	25Ar-75He	123	(291)
6	2519/5083	5356	25Ar-75He	174	(412)

## DISCUSSION

### Mechanical Properties

The weld properties were most significantly affected by the filler metal composition for the range of weld parameters studied. In general, post-weld aging and reduced weld heat input slightly increased the strength and lowered the ductility of the weld metal.

As indicated in Figures 6 through 9, when welding 2519 to itself, the 2319 and 4145 weldments showed the highest yield and tensile strength. The 2319 had the better ductility of the two filler materials. The 4043 showed the largest percent reduction of area, but the as-welded percent elongation was slightly lower than that of the 2319. The yield and ultimate tensile strength of the 4043 weldments was about 13% lower than that of the 2319 or the 4145.

In the tensile test results, almost all of the yielding and fracturing occur in the weld metal. The tensile specimens were machined from the center of the plates so that the root bead was primarily being tested. Because of the small size of the relatively soft weld region, the use of a 2" gauge length contributed to the low overall percent elongation values. The soft weld metal is ductile as evidenced by the larger percent reduction of area values.

Welding dissimilar joints between 2519 and 5083 aluminum alloys is not normally recommended by Alcoa and military specification MIL-A-46192. Nevertheless, welds were deposited on dissimilar metal joints of 19-mm (3/4") thick 2519 to 5083 using 2319, 4043, 4145, and 5356 aluminum filler metal alloys.

Upon welding 2519 to 5083, the 4043 aluminum developed excellent as-welded strength as shown in Figure 10. The tensile strength of the 2319 and 4145 filler metal welds were comparable to those of the 4043 filler metal. The 4043 has the best combination of strength and ductility when welding 2519 to 5083 of all the filler materials studied. It is possible that the dilution of magnesium from the 5083 into the 4043 filler metal is responsible for the increased strength of 4043 when welding 2519 to 5083. The 5356 filler material had surprisingly good ductility but provided the lowest strength weld joints. The amount of hot cracking encountered when using the 5356 renders this filler metal unacceptable.

The hot cracking susceptibilities of the weld metal and HAZ are known to be functions of both mechanical and metallurgical factors. External restraint, weld bead shape and size are important for mechanical aspects while the dendritic morphology and solidus/liquidus temperature range are the major metallurgical contributors to hot cracking.

Varestraint testing showed that the 4XXX series filler metals exhibit the least amount of hot cracking. This is due to the fact that the added elements will move the overall weld composition closer to the eutectic point, thus reducing the solidus/liquidus temperature range.

The welds made with 2319 did not reveal any hot cracking visually or radiographically. However, fractured tensile specimens of 2519 welded to 5083 using 2319 did show some slight regions of solidification cracking. This amount of cracking was not evidenced in the fractured specimens of 2519 welded to itself with 2319.

The CVN tests were not only performed in order to characterize 2519 weldments, but were also intended to help understand the welding parameters needed to fabricate weldments that can pass the ballistic shock test in MIL-STD-1946.

Due to the inability to properly place HAZ notches in this present study, we were unable to successfully use CVN testing to understand ballistic shock. However, a number of points can be made: under slow loading, the base metal is stronger, harder, and more ductile than the weld metal; under CVN testing, the base metal is weaker than the weld metal. Due to hardness traverse results, it is probable that there exists, near the fusion line or HAZ of remelted welds, a region of lowest impact resistance at the hardest region. It is this region which should fail earliest during the ballistic shock test.

## Fractography

Fractured surfaces of tensile, CVN, and ballistic specimens were examined with a SEM. The slow strain rate tensile tests all fractured in the weld metal which had the lowest hardness and lowest yield strength (in comparison to the fusion line, HAZ, and base metal). All fractures indicated a ductile mode of crack propagation (microvoid coalescence) as illustrated in Figure 21. The microvoids mostly initiated at  $\text{CuAl}_2$  precipitates.

All of the weld metal contained porosity which formed during solidification as evidenced by the dendrite arms shown in Figure 22. Previous research has shown that porosity will only affect the tensile properties by lowering the cross-sectional area. However, excess porosity may influence CVN properties. The fractured surfaces of the 4145 weldments which exhibited low CVN values all contained excessive porosity. In retrospect, this was due to receiving a bad spool of 4145 filler wire. Replacing the spool resulted in substantially less porosity. Unfortunately, as of the writing of this report, we did not test the CVN properties of the new 4145 weldments.

The CVN impact specimens also failed by ductile microvoid coalescence (MVC). Because of the difficulty in correctly placing a notch at the proper location on the fusion line or HAZ, CVN specimens were made with notches in the weld area only. Thus, it is difficult to use the CVN values to predict the results of ballistic tests.

The ballistic fractures seem to follow the weld fusion line as shown in Figure 2. Recall from Figure 18 that the inter-pass fusion line exhibits the highest hardness (which might also have the lowest impact resistance). However, even this area exhibited primarily ductile MVC fracture.

To date, CVN and ballistic shock test results have not been successfully correlated. This is possibly due to the large difference in impact velocities: about 5 ft/sec for CVN impact tests and 700 to 1000 ft/sec for ballistic shock tests (depending on the thickness). Another difference is that the CVN specimen has a notch and the ballistic specimen does not.

The ability to correlate CVN, small scale tests, and the MIL-STD-1946 ballistic shock test will be studied in a future research project.

### Weld Heat Input

The weld heat input was found to affect the primary dendrite arm spacing (DAS). A 36% reduction of DAS (from  $9.1 \times 10^{-6}$  m to  $6.7 \times 10^{-6}$  m) occurred when the heat input was reduced from 994 J/mm to 394 J/mm. It is documented in prior solidification studies<sup>4</sup> that aluminum alloys having reduced DAS developed better strength and toughness. Similarly, in this investigation, the reduction of DAS resulted in (1) slightly increased weld metal yield strength (Figure 7) and hardness both in the as-welded and post-weld aged conditions and (2) reduced volume of interdendritic second phase precipitation after welding. The reduced heat input (Schedule B) welds required 10 passes compared to only 8 passes (Schedule A) to complete a full penetration weld on 19-mm (3/4") thick plate.

Unfortunately, the refined DAS probably does not affect the properties enough to offset the added production costs of using a lower heat input. Additionally, the smaller weld beads make it more difficult to properly align the weld joint, and therefore lack of fusion may become a problem. It must be noted that heat input studies did not cover the entire range of heat inputs being used for aluminum vehicle production. Higher heat inputs (up to 80 kJ/in.) are now being studied.

Microstructures of welds deposited on 2519 with 2319 exhibited typical dendritic morphologies. At the weld metal/base metal interface, shown in Figure 23, an equiaxed grain structure with dispersed  $\text{CuAl}_2$  precipitates in the grain boundaries formed as a result of partial melting in the solidus/liquidus temperature range. The effect of this partially melted region on the fracture path is still under investigation at the time of this writing.

### Shielding Gas Composition

In the past weldability studies of 2519 aluminum,<sup>1,3</sup> virtually all GMAW has been performed with pure argon shielding gas. However, the bead surface profile and "finger" or "spike" penetration of GMAW with pure argon increased the incidence of lack of fusion defects, particularly in root passes. The use of a 25Ar-75He gas mixture provided several advantages over pure argon for welding the 19-mm (3/4") and 32-mm (1-1/4") thick plates in this investigation. Since pure argon produced a "spike" type penetration pattern, great care had to be taken to ensure that the land of the root pass was fully fused. A slight misalignment of the welding torch could cause a lack of fusion defect along the land. The 25Ar-75He shielding gas welds, however, developed greater side wall penetration than those shielded with pure argon and ensured excellent fusion of the seam during the root pass despite any misalignments of the torch. In addition, it has been reported that Ar/He mixtures result in less porosity than pure argon.<sup>5</sup>

It must be noted, however, that argon is considerably less expensive than helium, and in most production applications pure argon is used. If a high heat input is used, the larger weld bead will probably not have the lack of fusion problems that were encountered with the lower heat input parameters listed in Table 4.

5. FLEMING, M.C. *Solidification Processing*. McGraw-Hill, New York, 1976.

## Deposition Rate

Filler metal composition and shielding gas composition substantially affected the deposition rate during GMAW of 2519 aluminum as summarized in Table 7. Apparently, deposition rate increases (at constant heat input) as the electrical resistivity of the filler metal increases. For example, the deposition rate as measured by wire feed rate, for the 2319 filler containing Al and Cu is substantially less than that for 5356 filler containing Al and large amounts of Mg. The greater electrical resistivity of the 5356 filler permitted an increase in  $I^2R$  preheating of the wire between the contact tube and the arc.

Similarly, the deposition rate of a given filler metal (at constant heat input) increased with increasing electrical resistivity or thermal conductivity of the shielding gas plasma. For example, a 30% increase in wire feed rate was achieved by replacing 100Ar with 25Ar-75He (and maintaining a constant current) as displayed in Table 7.

Another way to view the effect of changing shielding gases is to leave the wire feed rate constant, and determine the change in current. When 100Ar is replaced with 25Ar-75He, the current drops from 350 amps to 265 amps (at 3/4" stick-out, 26 volts, and 158 mm/s wire feed rate). This results in an increase in apparent arc resistivity from 0.074 ohms ( $26/350$ ) to 0.098 ohms ( $26/265$ ) when changing to 25Ar-75He. The mechanism by which deposition rate changes as a function of shielding gas and filler metal resistivity is not well understood.

## Post-Weld Heat Treatment

Welds made with 2319 filler metal were always responsive to post-weld heat treatment to some extent. The weld metal deposited on the 2519 plates was virtually as precipitation hardenable as the 2519 base metal as shown in Figure 24. Precipitation hardening reactions taking place in the dissimilar metal welds between 2319 and 5083 aluminum alloys were a function of Cu content. The weld passes adjacent to the 2519 side of the weld joint responded to heat treatment almost as well as the 2519 base metal. The weld passes adjacent to the 5083 side of the weld exhibited a somewhat weaker response to precipitation hardening (Figure 24). The 5083 aluminum displayed very little hardening since the Mg in the 5083 is unable to form coherent zones upon aging as does the Cu in the 2319 and 2519 aluminum alloys.

The post-weld aging treatments did not increase the strength of 2XXX series weldments as much as originally anticipated. In response to this, a more detailed aging study was performed. It was found that natural aging at room temperature is nearly as effective as artificial aging at 400°F as shown in Figure 20. Natural aging may also account for the fact that microhardness traverses did not distinguish a solution heat treated condition in the weld zone as was initially suspected.

The low heat input Weld #1 had greater as-quenched hardness and greater response to precipitation hardening than the medium heat input welds as shown in Figure 25. This is generally true since the low heat input produces a finer dendrite arm spacing and permits shorter diffusion distances to achieve the compositional changes required for the precipitation hardening reactions.

## Hardness

Knoop hardness traces were measured in order to understand the microstructural hardening mechanisms and their effects on failure location. Although a thorough characterization is inappropriate at this time, a number of plausible inferences can be drawn.

The 2519 base metal immediately adjacent to the weld bead is heated above the recrystallization temperature. Outside of that region, the material becomes overaged and large precipitates form with a corresponding decrease in strength. This explains the shape of the hardness traces in Figures 16 and 17 which show an increase in hardness adjacent to the weld (on the 2519 side) followed by a region of decreased hardness before the base metal returns to its unwelded hardness of approximately HK 143.

The 5083, which is not a precipitation hardenable alloy, does not show an increase in hardness, but only a decrease in the weld vicinity. This is a result of the agglomeration of the beta precipitate phase due to the heat of welding.

The strength and hardness of the weld metal are primarily functions of composition. Figures 16a through 16c show the weld metal in a condition similar to being solution heat treated and naturally aged. The 4043, which has the least amount of copper, also has the lowest hardness and strength. Although the 2319 has the most copper, it is not as hard as the 4145 which is alloyed with silicon and magnesium (like the 4043).

Magnesium, diluted into the weld from 5083 (when welding 2519 to 5083), was found to increase the hardness of all three filler metals as shown in Figures 19a through 19c. This accounts for the fact that 4043 is stronger when welding 2519 to 5083 than when welding 2519 to itself. The fact that this dilution does not increase the strength of the 4145, however, indicates that there is a complex interaction of the alloying elements that is not presently understood. A consumables development program for welding 2519 may be appropriate at a later date.

The heat of a temper bead increases the hardness of all three filler metals slightly (approximately 5 on the HK scale). It also decreases the hardness of the initially recrystallized zone so that the difference in hardness is much less than that of a single pass weld. However, the weld bead next to the fusion line of the temper bead and area immediately adjacent to the temper bead undergoes recrystallization. The increase in hardness due to this second recrystallization is proportional to the amount of copper in the weld bead. This is responsible for the hardness spike found in Figure 18.

This increased hardness region along the boundary from weld bead to weld bead in a multipass weld may play a role in tensile and ballistic failures. Figure 26 shows a cross section of a fractured tensile specimen. As can be seen, the fracture follows the soft region adjacent to the hard region between passes. The hard region will even turn the crack 90° to stay in the soft region rather than cross through that hard region.

Another postulate now being studied is that low melting point eutectic regions may be found at the grain boundaries in the partially melted zone adjacent to the fusion line. The areas may promote crack propagation and failure upon ballistic loading. The partially melted zone is right next to the hard recrystallized zone which may also be a brittle region during ballistic testing.

## CONCLUSIONS

The following conclusions can be made based on the data obtained during this investigation:

1. The filler metals which have the best as-welded strength when welding 2519-T87 to itself are: 2319 and 4145. Of these, 2319 has the better ductility.
2. The filler metal which has the highest as-welded strength and ductility when welding 2519-T87 to 5083-H131 is 4043.
3. Reduced heat input, type of shielding gas, plate thickness, and post-weld heat treatment have a minor influence on the weld strength and ductility (for the materials and parameters studied).
4. Hot cracking can occur when welding 2519-T87 to 5083-H131. V restraint tests show that 4043 and 4145 are resistant to hot cracking, 2319 can crack under very high restraint, and 5356 will crack even under low restraint.
5. The presence of a temper bead changes the hardness profile across the weldment. The effect of the temper bead decreases the difference in hardness from the HAZ to the weld metal and may increase ballistic performance.
6. Weldments of 2519-T87 welded to itself using 2319 filler material can pass ballistic qualification to MIL-STD-1946. Previously reported ballistic failures of this material were found to be invalidly tested.

## FOLLOW-ON RESEARCH

A number of follow-on tests can be designed based on the presented results:

1. Ballistic weldments will be fabricated and tested using various filler materials, joint geometries, and high heat inputs. The 4043 and 2319 filler metals seem to be the most promising. As of the writing of this report, 26 weldments are being fabricated to be tested in accordance with the ballistic shock test in MIL-STD-1946.
2. CVN specimens can be heated with a Gleeble 1500 to simulate the HAZ properties of interest. These specimens will be machined to have the notch in the proper microstructure.
3. The effect of high heat input (40 to 60 kJ/in.) welds will be studied in order to more accurately reflect what presently is taking place during production of aluminum armor weldments.
4. The effect of temper beads will be further studied. The weldments will be mechanically tested in order to compare the results to the previously obtained data.

## ACKNOWLEDGMENTS

The authors would like to express their appreciation to the Army Research Office program which enabled Jack Devletian to spend his sabbatical here at MTL. Thanks to the Massachusetts Institute of Technology Co-op program for providing Sandra DeVincent the opportunity of working at MTL.

Most importantly, the authors would like to recognize the continuing efforts of the MTL welding laboratory technicians: James Catalano, Donald Hassett, and Attilio Santoro. Their experience, assistance, and foresight in having all the proper equipment and supplies proved to be invaluable.

The authors would also like to thank Sin-Jang Chen and David W. Yu, graduate students at the Oregon Graduate Center, for spending their time machining samples and performing the varentstraint tests.

Thanks to Eugenio DeLuca for providing details on the ballistic testing of weldments.

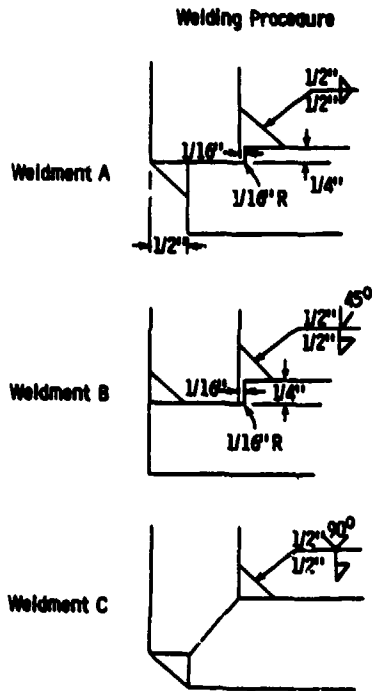


Figure 1. Corner joint weld geometries. Joints A and B passed ballistic qualification to MIL-STD-1946.

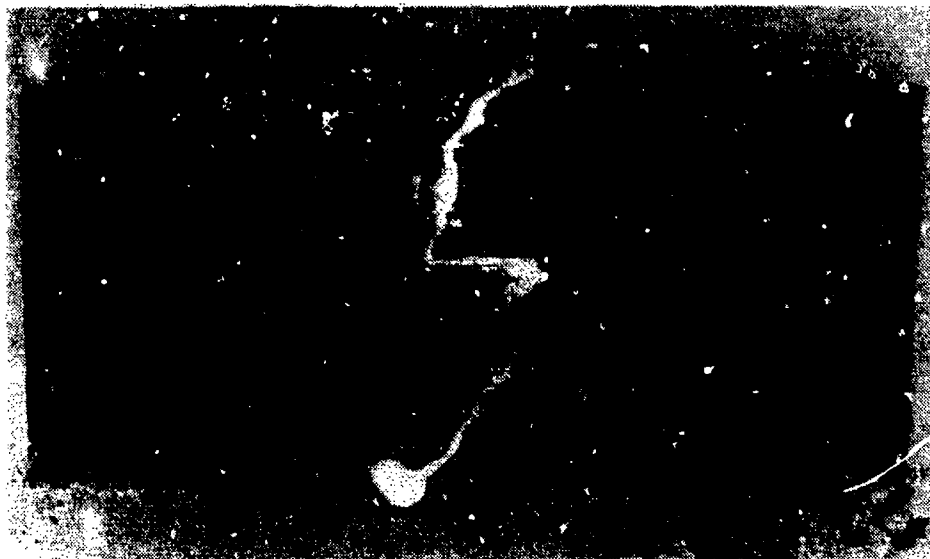
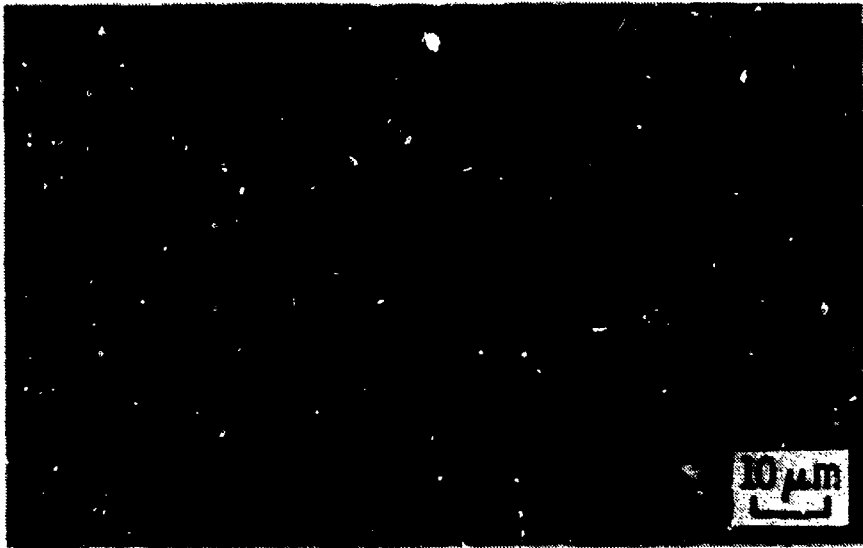


Figure 2. Micrograph of ballistic shock test specimen of 2519-T87 welded to itself using 2319 filler metal, showing crack propagation near the fusion line, Mag. 2X.



**Figure 3. Fractograph of ballistic shock test specimen of 2519-T87 welded to itself using 2319 filler metal, indicating a ductile fracture mode, Mag. 1000X.**



**Figure 4. Fractograph of ballistic shock test specimen of 2519-T87 welded to itself using 2219 filler metal, displaying brittle areas surrounded by ductile dimpling, Mag. 500X.**

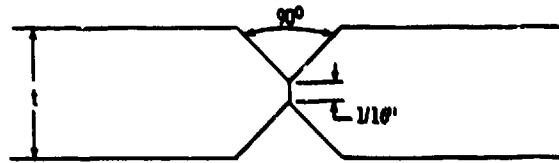


Figure 5. Double-V groove weld joint geometry used for mechanical specimens.

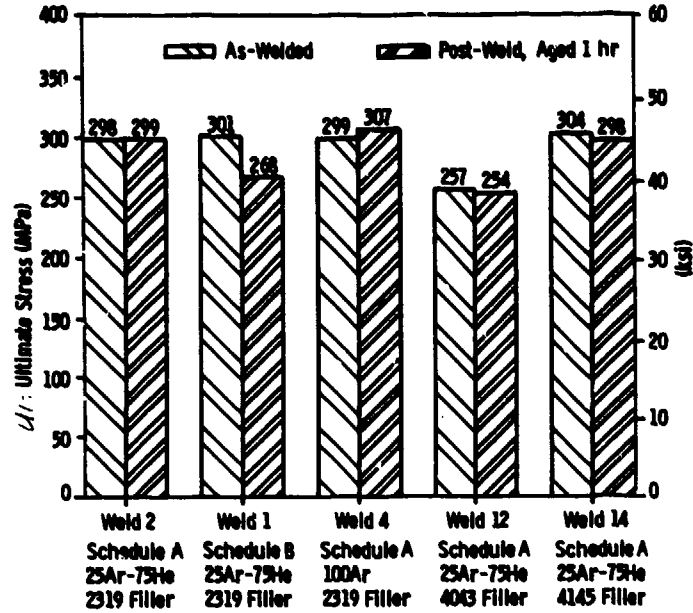


Figure 6. Ultimate tensile strength of 2519-T87 to 2519-T87 weldments.

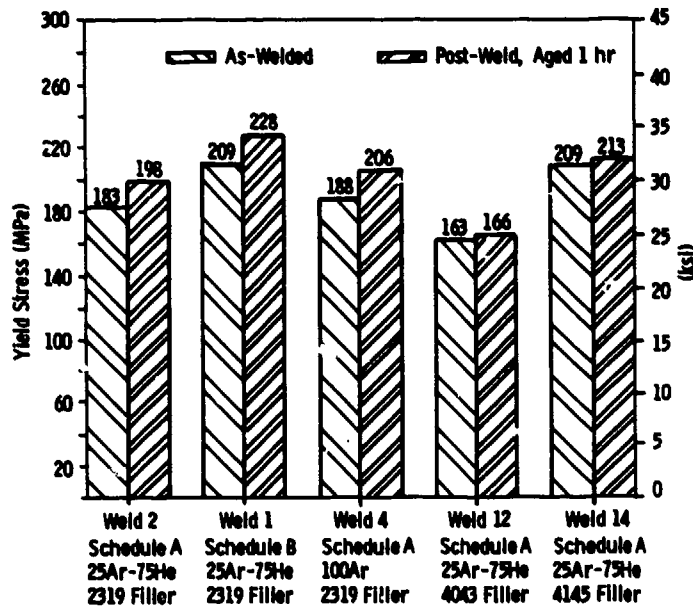


Figure 7. Two percent offset yield strength of 2519-T87 to 2519-T87 weldments.

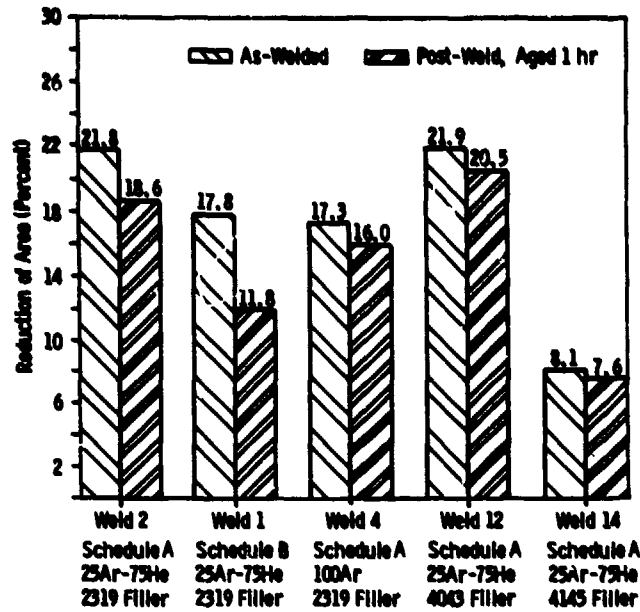


Figure 8. Percent reduction of area of 2519-T87 to 2519-T87 weldments.

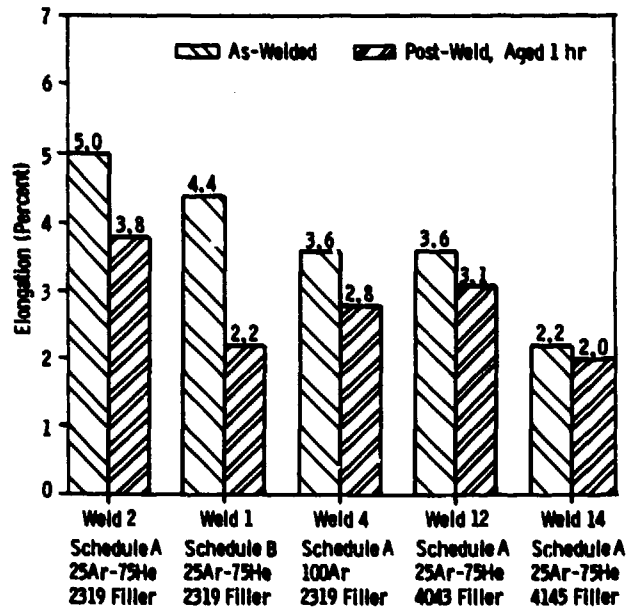


Figure 9. Percent elongation of 2519-T87 to 2519-T87 weldments.

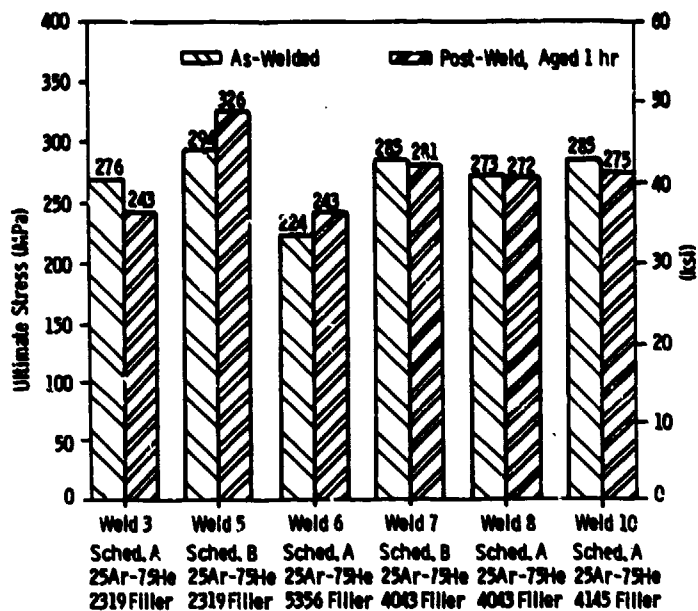


Figure 10. Ultimate tensile strength of 2519-T87 to 5083-H131 weldments.

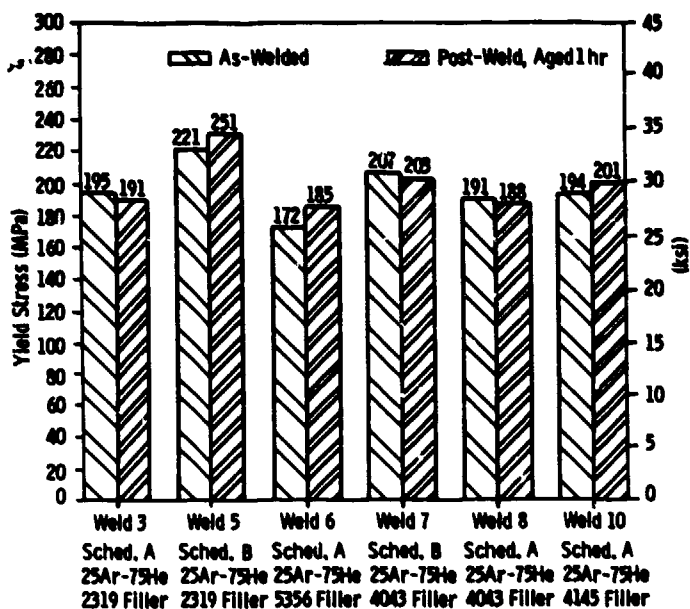


Figure 11. Two percent offset yield strength of 2519-T87 to 5083-H131 weldments.

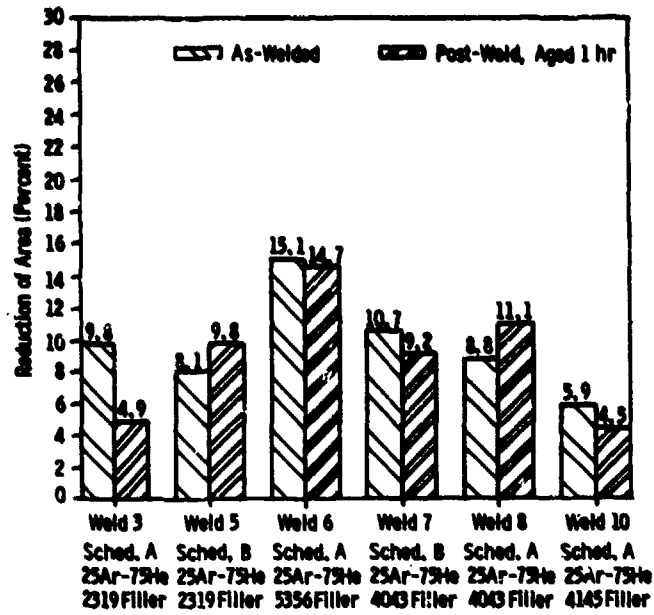


Figure 12. Percent reduction of area of 2519-T87 to 5083-H131 weldments.

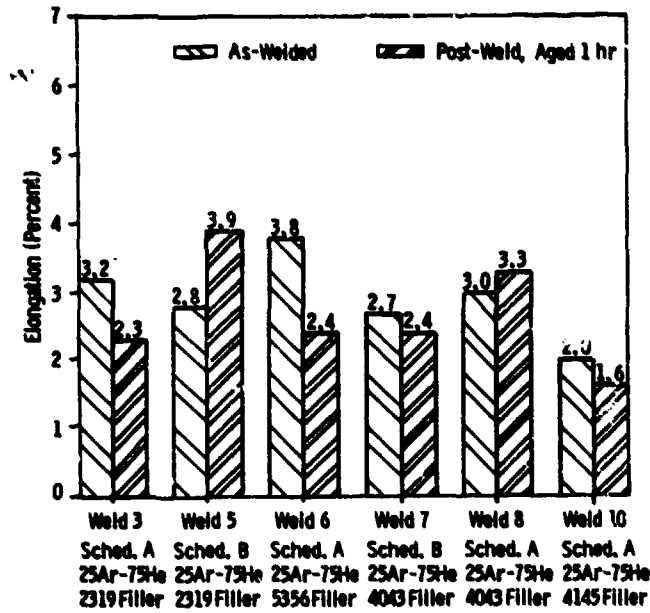


Figure 13. Percent elongation of 2519-T87 to 5083-H131 weldments.

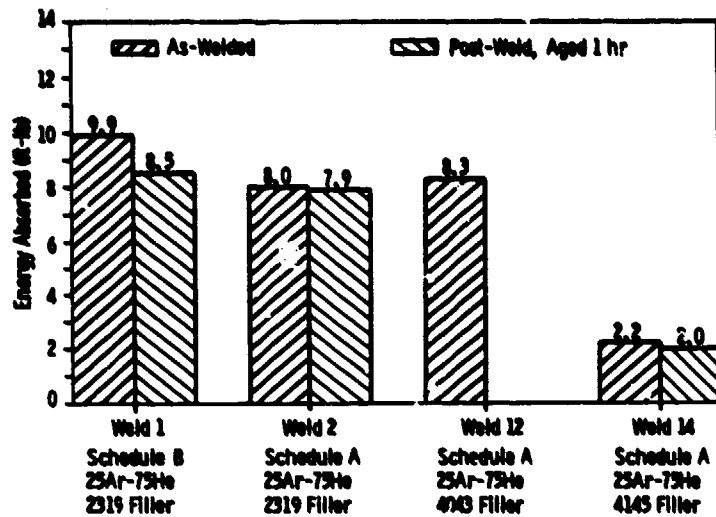


Figure 14. Charpy V-notch impact test results of 2519-T87 to 2519-T87 weldments.

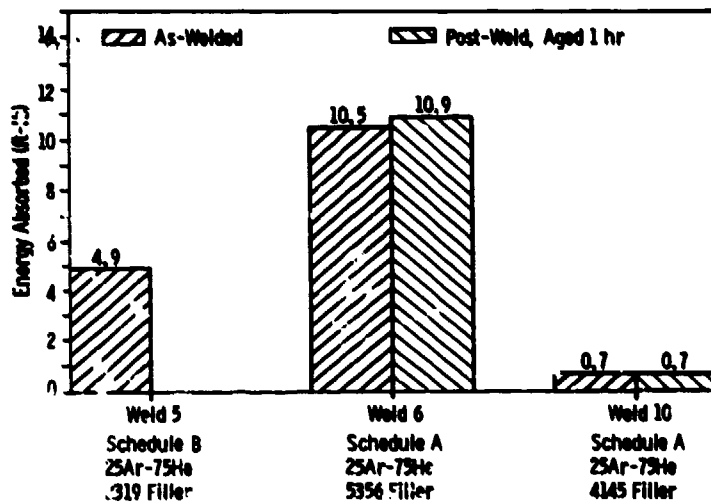


Figure 15. Charpy V-notch impact test results of 2519-T87 to 6083-H131 weldments.

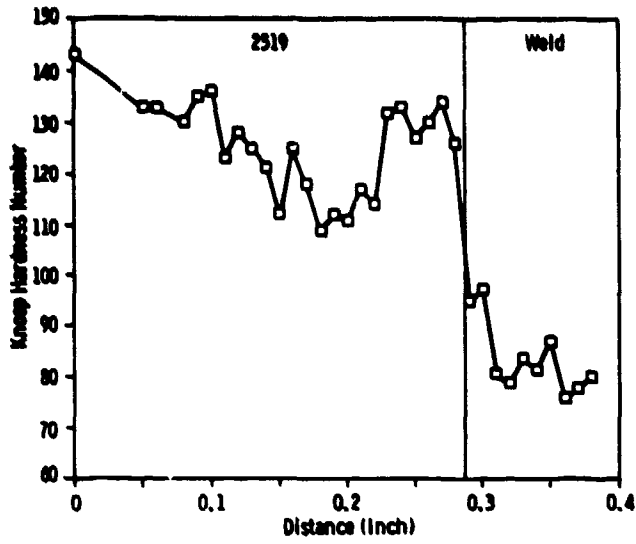


Figure 16a. Knoop hardness traverse of bead on plate (2519-T87) weldment using 2319 filler metal.

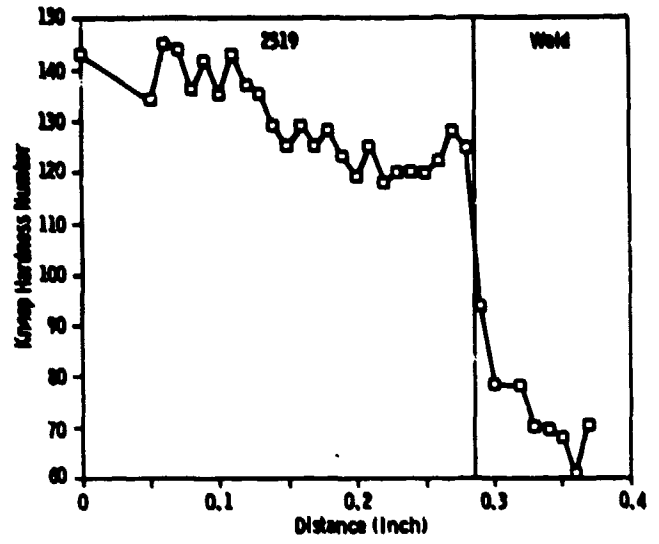


Figure 16b. Knoop hardness traverse of bead on plate (2519-T87) weldment using 4043 filler metal.

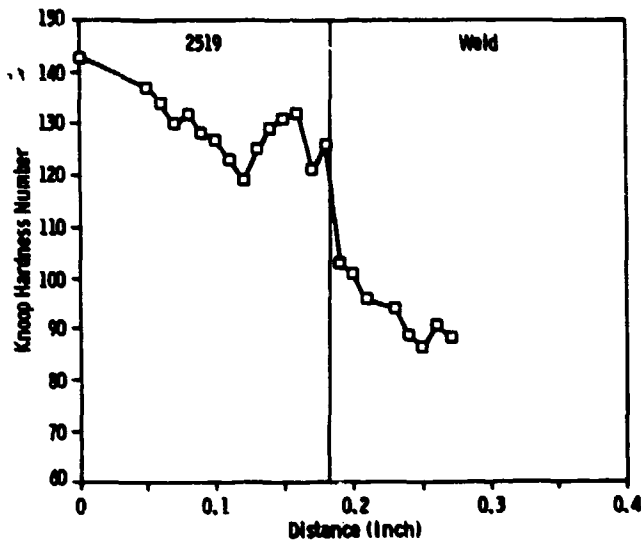


Figure 16c. Knoop hardness traverse of bead on plate (2519-T87) weldment using 4145 filler metal.

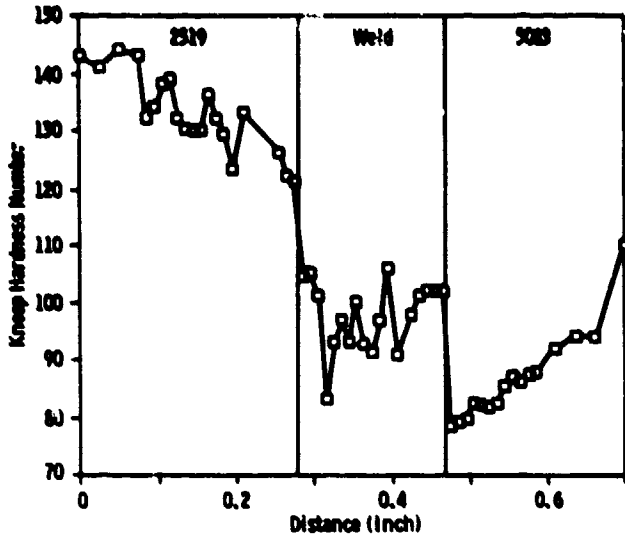


Figure 17a. Knoop hardness traverse of 2519-T87 to 5083-H131 root pass weldment using 2319 filler metal.

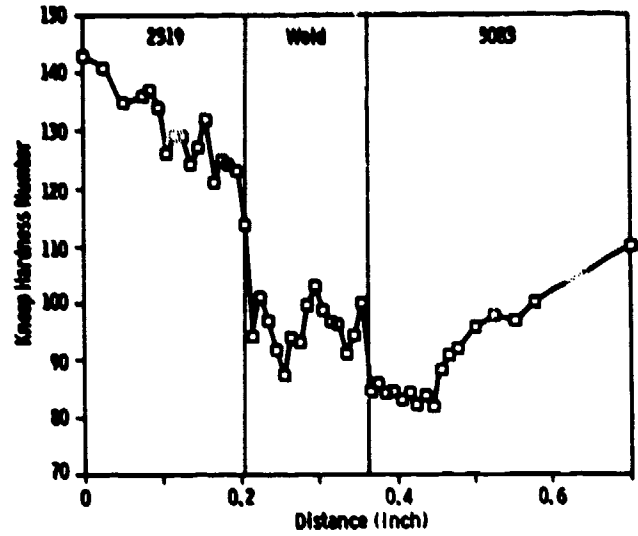


Figure 17b. Knoop hardness traverse of 2519-T87 to 5083-H131 root pass weldment using 4043 filler metal.

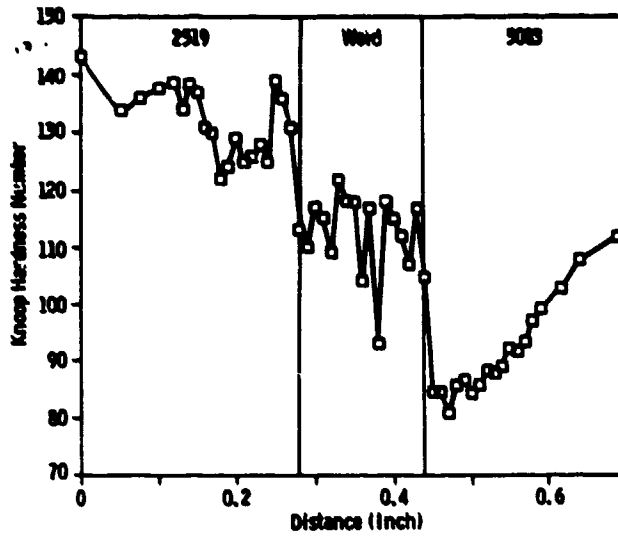


Figure 17c. Knoop hardness traverse of 2519-T87 to 5083-H131 root pass weldment using 4145 filler metal.

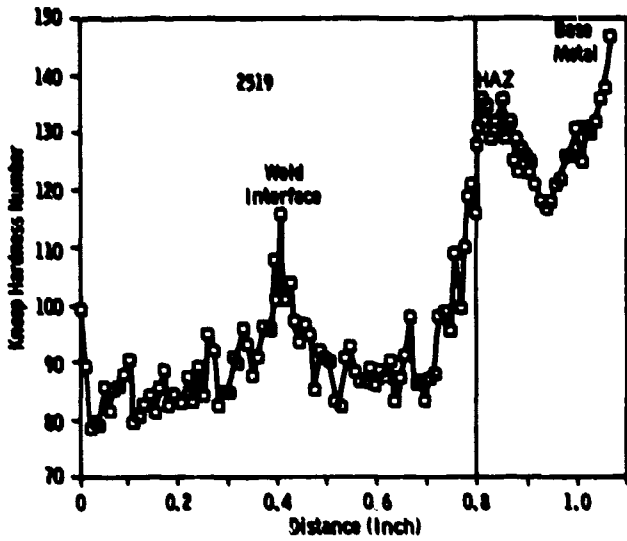


Figure 18. Knoop hardness traverse across a multipass weld (2519-T87 welded to itself with 2319).

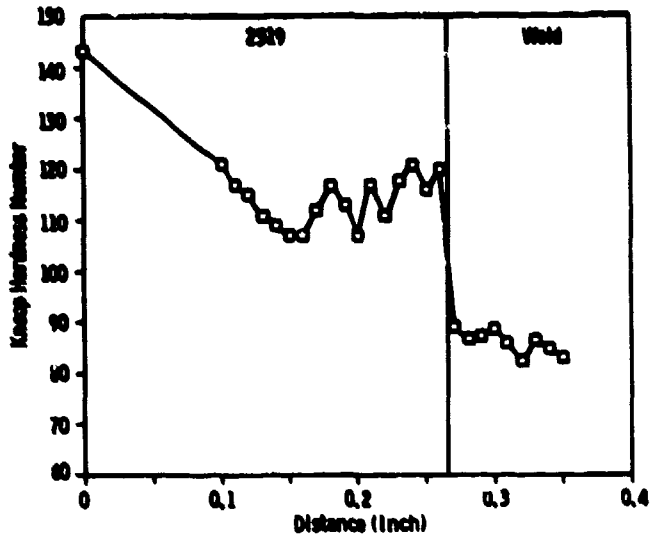


Figure 19a. Knoop hardness traverse of temper bead showing 2319 filler metal on 2519-T87.

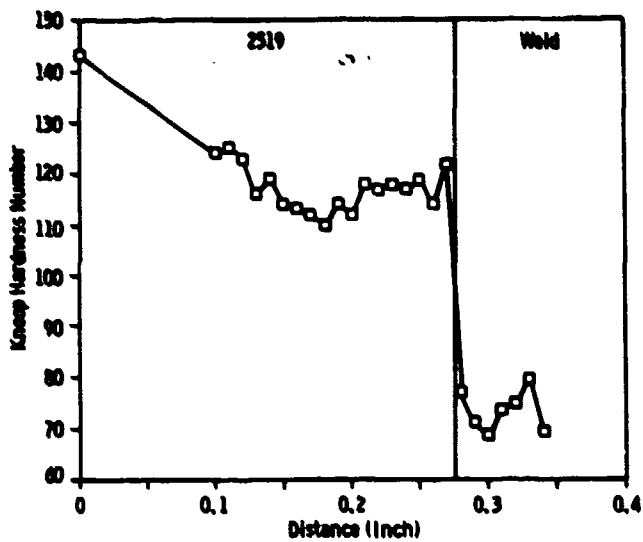


Figure 19b. Knoop hardness traverse of temper bead showing 4043 filler metal on 2519-T87.

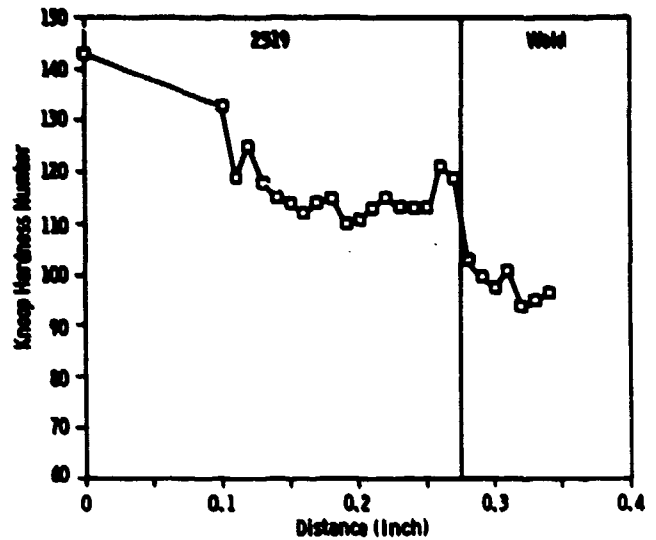


Figure 19c. Knoop hardness traverse of temper bead showing 4145 filler metal on 2519-T87.

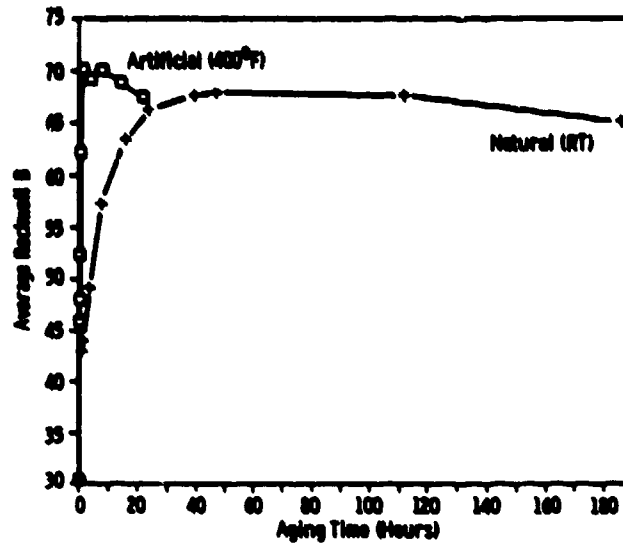


Figure 20. Effect of artificial and natural (room temperature) aging on solution heat treated 2519-T87 aluminum.



Figure 21. Fractograph of CVN specimen indicating a ductile mode of crack propagation, Mag. 1000X.

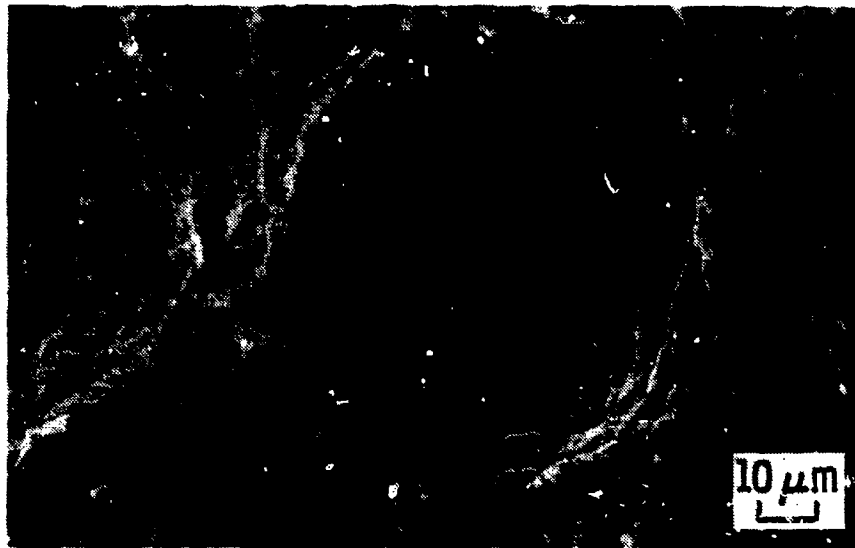


Figure 22. Fractograph of tensile specimen showing dendrite arms, Mag. 750X.

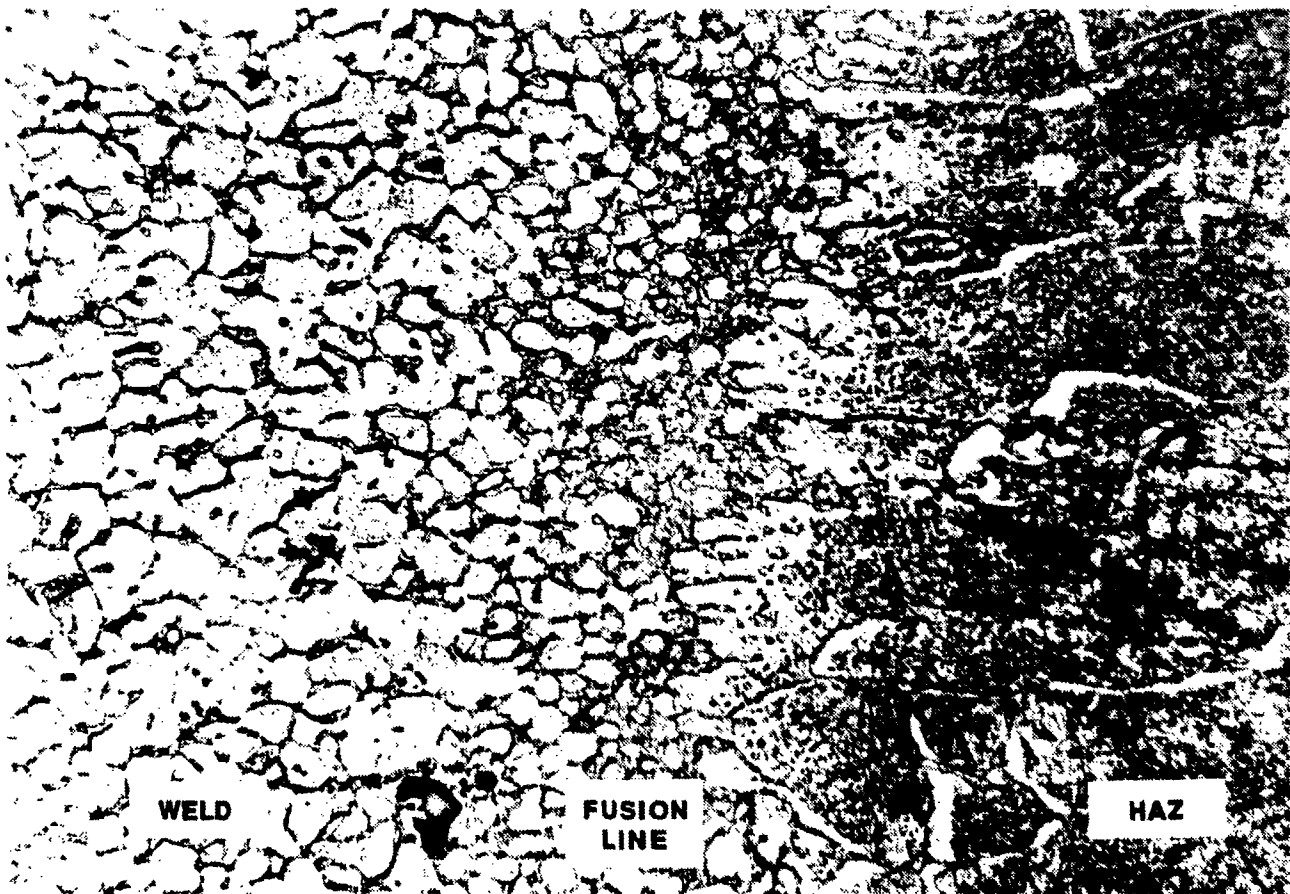


Figure 23. Micrograph of 2519-T87 to 2519-T87 weldment using 2319 filler metal, Mag. 500X.

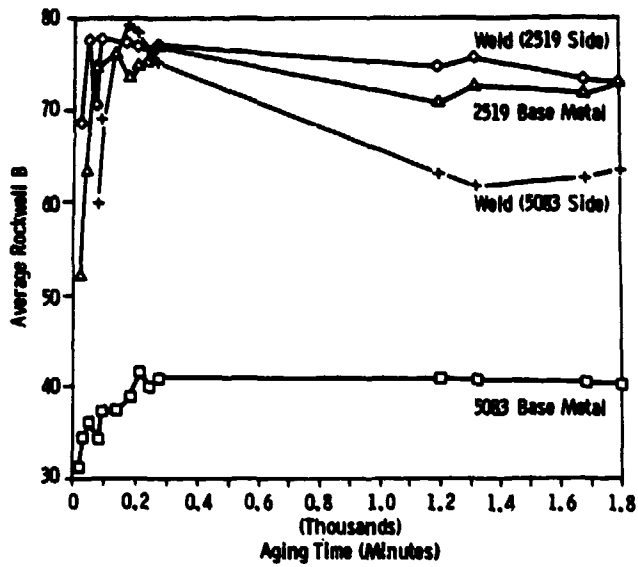


Figure 24. Effect of aging time on Rockwell B hardness of solution heat treated 2519-T87 to 5083-H131 weldments (using 2319 filler metal).

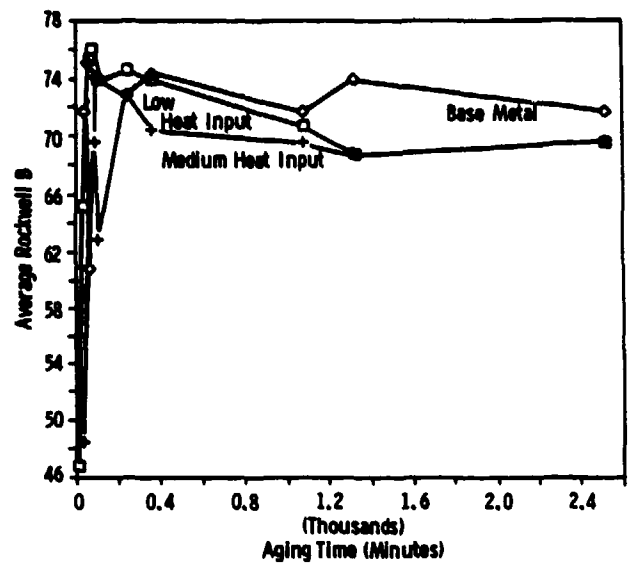


Figure 25. Effect of aging time on Rockwell B hardness of low and medium heat input, solution heat treated, 2519-T87 to 2519-T87 weldments (using 2319 filler metal).



Figure 26. Micrograph showing the fracture path in a tensile specimen of 2519-T87 welded to itself with 2319 filler metal, Mag. 4X.

DISTRIBUTION LIST

No. of Copies	To
1	Office of the Under Secretary of Defense for Research and Engineering, The Pentagon, Washington, DC 20301
	Commander, U.S. Army Laboratory Command, 2800 Powder Mill Road, Adelphi, MD 20783-1145
1	ATTN: AMSLC-IM-TL
	Commander, Defense Technical Information Center, Cameron Station, Building 5, 5010 Duke Street, Alexandria, VA 22304-6145
2	ATTN: DTIC-FDAC
	Metals and Ceramics Information Center, Battelle Columbus Laboratories, 505 King Avenue, Columbus, OH 43201
1	ATTN: Harold Mindlin
	Commander, Army Research Office, P.O. Box 12211, Research Triangle Park, NC 27709-2211
1	ATTN: Information Processing Office
	Commander, U.S. Army Materiel Command (AMC), 5001 Eisenhower Avenue, Alexandria, VA 22333
1	ATTN: AMCLD
	Commander, U.S. Army Materiel Systems Analysis Activity, Aberdeen Proving Ground, MD 21005
1	ATTN: AMXSY-MP, Director
	Commander, U.S. Army Missile Command, Redstone Scientific Information Center, Redstone Arsenal, AL 35898-5241
1	ATTN: AMSMI-RD-CS-R/Doc
	Commander, U.S. Army Armament, Munitions and Chemical Command, Dover, NJ 07801
2	ATTN: Technical Library
	Commander, U.S. Army Tank-Automotive Command, Warren, MI 48397-5000
1	ATTN: AMSTA-ZSK
2	AMSTA-TSL, Technical Library
1	AMSTA-RCK
	Commander, U.S. Army Foreign Science and Technology Center, 220 7th Street, N.E., Charlottesville, VA 22901
1	ATTN: Military Tech
	Director, Eustis Directorate, U.S. Army Air Mobility Research and Development Laboratory, Fort Eustis, VA 23604
1	ATTN: SAVDL-E-MOS (AVSCOM)
1	SAVDL-EU-TAP
	U.S. Army Aviation Training Library, Fort Rucker, AL 36360
1	ATTN: Building 5906--5907
	Commander, U.S. Army Aviation Systems Command, 4300 Goodfellow Boulevard, St. Louis, MO 63120
1	ATTN: AMDAV-EGX
1	AMDAV-EX, Mr. R. Lewis
1	AMDAV-EQ, Mr. Crawford
2	AMCPM-AAH-TM, Mr. R. Hubbard, Mr. B. J. Baskett
1	AMDAV-DS, Mr. W. McClane
	Naval Research Laboratory, Washington, DC 20375
1	ATTN: Code 5830
1	Code 2627

No. of Copies	To
1	Chief of Naval Research, Arlington, VA 22217 ATTN: Code 471
1	Director, Structural Mechanics Research, Office of Naval Research, 800 North Quincy Street, Arlington, VA 22203 ATTN: Dr. M. Perrone
1	Edward J. Morrissey, AFWAL/MLTE, Wright Patterson Air Force Base, OH 45433
1	Commander, U.S. Air Force Wright Aeronautical Laboratories, Wright-Patterson Air Force Base, OH 45433
1	ATTN: AFWAL/MLC
1	AFWAL/MLLP, D. M. Forney, Jr.
1	AFWAL/MLBC, Mr. Stanley Schulman
1	AFWAL/MLXE, A. Olevitch
1	National Aeronautics and Space Administration, Marshall Space Flight Center, Huntsville, AL 35812
1	ATTN: R. J. Schwinghammer, EH01, Dir, M&P Lab
1	Mr. W. A. Wilson, EH41, Bldg. 4612
1	Chief of Naval Research, Washington, DC 20350 ATTN: OP-987, Director
1	Aeronautical Systems Division (AFSC), Wright-Patterson Air Force Base, OH 45433
1	ATTN: ASD/ENFEF, D. C. Wight
1	ASD/ENFTV, D. J. Wallick
1	ASD/XRHD, G. B. Bennett
1	Air Force Armament Laboratory, Eglin Air Force Base, FL 32542 ATTN: AFATL/DLYA, V. D. Thornton
1	Air Force Flight Dynamics Laboratory, Wright-Patterson Air Force Base, OH 45433
1	ATTN: AFFDL/FIES, J. Sparks
1	AFFDL/FIES, J. Hodges
1	AFFDL/TST, Library
1	Air Force Test and Evaluation Center, Kirtland Air Force Base, NM 87115 ATTN: AFTEC-JT
1	NASA - Ames Research Center, Army Air Mobility Research and Development Laboratory, Mail Stop 207-5, Moffett Field, CA 94035 ATTN: SAVDL-AS-X, F. H. Immen
1	NASA - Johnson Spacecraft Center, Houston, TX 77058 ATTN: JM6
1	ES-5
1	Naval Air Development Center, Warminster, PA 18974 ATTN: Code 063
1	Code 6062
1	Naval Air System Command, Department of the Navy, Washington, DC 20360
1	ATTN: AIR-03PAF
1	AIR-5203
1	AIR-5164J
1	AIR-530313
1	Naval Post Graduate School, Monterey, CA 93948 ATTN: Code 57BP, R. E. Ball

No. of Copies	To
1 1	Naval Surface Weapons Center, Dahlgren Laboratory, Dahlgren, VA 22448 ATTN: Code G-54, Mr. J. Hall Code G-54, Dr. B. Smith
1	Commander, Rock Island Arsenal, Rock Island, IL 61299 ATTN: AMSAR-PPV
1	Armament Systems, Inc., 712-F North Valley, Anaheim, CA 92801 ATTN: J. Musch
1	Beech Aircraft Corporation, 9709 E. Central Avenue, Wichita, KS 67206 ATTN: Engineering Library
1	Bell Helicopter Company, A Textron Company, P.O. Box 482, Fort Worth, TX 76101 ATTN: J. R. Johnson
1	Boeing Vertol Company, A Division of the Boeing Company, P.O. Box 16858, Philadelphia, Philadelphia, PA 19142 ATTN: J. E. Gonsalves, M/S P32-19
1	Cessna Military, P.O. Box 7704, Wichita, KS 67277-7704
1	Fairchild Industries, Inc., Fairchild Republic Company, Conklin Street, Farmingdale, Long Island, NY 11735 ATTN: Engineering Library, G. A. Mauter
1	FMC Corporation, Central Engineering Labs, 1185 Coleman Avenue, Box 80, Santa Clara, CA 95052 ATTN: Gary L. Boerman
1	FMC Corporation, Ordnance Division, 1105 Coleman Avenue, Box 1201, San Jose, CA 95108 ATTN: William H. Altergott
1	General Dynamics Corporation, Convair Division, P.O. Box 80877, San Diego, CA 92138 ATTN: Research Library
1	Gruman Aerospace Corporation, South Oyster Bay Road, Bethpage, NY 11714 ATTN: Technical Information Center, J. Davis
1 1 1	McDonnell Douglas Helicopter Co., 5000 East McDowell Road Mesa, AZ 85205-9797 ATTN: Library Mr. A. Hirko Mr. L. Soffa
1	IIT Research Institute, 10 West 35th Street, Chicago, IL 60616 ATTN: K. McKee
1	Kaman Aerospace Corporation, Old Winsor Road, Bloomfield, CT 06002 ATTN: H. E. Showalter
1	Lockheed-California Company, A Division of Lockheed Aircraft Corporation, Burbank, CA 91503 ATTN: Technological Information Center, 84-40, U-35, A-1
1	Vought Corporation, P.O. Box 5907, Dallas, TX 75232 ATTN: D. M. Reedy, 2-30110
1	Martin Marietta Corporation, Orlando Division, P.O. Box 5837, Orlando, FL 32805 ATTN: Library, M. C. Griffith

No. of Copies	To
1	McDonnell Douglas Corporation, 3855 Lakewood Boulevard, Long Beach, CA 90846 ATTN: Technical Library, CI 290/36-84
1	Northrop Corporation, Aircraft Division, 3901 W. Broadway, Hawthorne, CA 90250 ATTN: Mgr. Library Services, H. W. Jones
1	Parker Haffifin, 14300 Alton Pkwy., Irvine, CA 92718-1814 ATTN: C. Beneker
1	Sikorsky Aircraft, A Division of United Aircraft Corporation, Main Street, Stratford, CT 06601 ATTN: Mel Schwartz, Chief of Metals
1	Teledyne CAE, 1330 Laskey Road, Toledo, OH 43697 ATTN: Librarian
1	Georgia Institute of Technology, School of Mechanical Engineering, Atlanta, GA 30332 ATTN: Mechanical Engineering Library
1	Lukens Steel Company, Coateville, PA 19320 ATTN: Dr. E. Hamburg
1	Mr. A. Wilson
1	Republic Steel Corporation, 410 Oberlin Avenue SW, Massillon, OH 44646 ATTN: Mr. R. Sweeney
1	Mr. W. H. Brechtel
1	Mr. T. M. Costello
1	L. Raymond Associates, P.O. Box 7925, Newport Beach CA 92658-7925 ATTN: Dr. L. Raymond
1	Ingersoll Rand Oilfield Products Division, P.O. Box 1101, Pampa, TX 79065 ATTN: Mr. W. L. Hallerberg
1	Brown University, Division of Engineering, Providence, RI 02912 ATTN: Prof. J. Duffy
1	SRI International, 333 Ravenswood Avenue, Menlo Park, CA 94025 ATTN: Dr. D. Shockey
1	Illinois Institute of Technology, Metallurgical and Materials Engineering Department, Chicago, IL 60616 ATTN: Dr. Norman Breyer
1	Roger Stanton, SMCAR-AET-M, Bldg. 355, Picatinny Arsenal, Dover, NJ 07806-5000
2	Dr. Jack H. Devletian, Department of Materials Science and Engineering, Oregon Graduate Center, 19600 N.W. Van Neumann Drive, Beaverton, OR 97006-1999
1	Dr. Thomas Eagar, Department of Materials Science and Engineering, MIT, Cambridge, MA 02139
1	Dr. Steven A. Gedeon, via delle industrie, 39, 30175 Porto Marghera-ve, Italy
2	Director, U.S. Army Materials Technology Laboratory, Watertown, MA 02172-0001 ATTN: SLCMT-TML
3	Authors

U.S. Army Materials Technology Laboratory  
Watertown, Massachusetts 02172-0001  
WELDABILITY OF 2519-T87 ALUMINUM  
ALLOY - Jack H. Devletian, Sandra M.  
DeVincent, and Steven A. Gedeon

Technical Report MTL TR 88-47, December 1988, 28 pp-  
illus-tables, D/A Project 16162105AH84, AMCMS  
Code 612105.H84

Test results show that 2519-T87 is weldable to itself and to 5083-H131. A wide variety of filler metals, weld parameters, and post-weld heat treatments were studied to determine the effect on weld mechanical properties, hot crack susceptibility, microstructure, and ballistic integrity. Previously reported 2519-T87 weldment ballistic failures have been discovered to be invalid. New ballistic weldments of 2519-T87 welded to itself were successfully qualified to the shock test in MIL-STD-1946.

AD UNCLASSIFIED  
UNLIMITED DISTRIBUTION

Key Words

Weldability  
Aluminum alloys  
Mechanical properties

U.S. Army Materials Technology Laboratory  
Watertown, Massachusetts 02172-0001  
WELDABILITY OF 2519-T87 ALUMINUM  
ALLOY - Jack H. Devletian, Sandra M.  
DeVincent, and Steven A. Gedeon

Technical Report MTL TR 88-47, December 1988, 28 pp-  
illus-tables, D/A Project 16162105AH84, AMCMS  
Code 612105.H84

Test results show that 2519-T87 is weldable to itself and to 5083-H131. A wide variety of filler metals, weld parameters, and post-weld heat treatments were studied to determine the effect on weld mechanical properties, hot crack susceptibility, microstructure, and ballistic integrity. Previously reported 2519-T87 weldment ballistic failures have been discovered to be invalid. New ballistic weldments of 2519-T87 welded to itself were successfully qualified to the shock test in MIL-STD-1946.

AD UNCLASSIFIED  
UNLIMITED DISTRIBUTION

Key Words

Weldability  
Aluminum alloys  
Mechanical properties

U.S. Army Materials Technology Laboratory  
Watertown, Massachusetts 02172-0001  
WELDABILITY OF 2519-T87 ALUMINUM  
ALLOY - Jack H. Devletian, Sandra M.  
DeVincent, and Steven A. Gedeon

Technical Report MTL TR 88-47, December 1988, 28 pp-  
illus-tables, D/A Project 16162105AH84, AMCMS  
Code 612105.H84

Test results show that 2519-T87 is weldable to itself and to 5083-H131. A wide variety of filler metals, weld parameters, and post-weld heat treatments were studied to determine the effect on weld mechanical properties, hot crack susceptibility, microstructure, and ballistic integrity. Previously reported 2519-T87 weldment ballistic failures have been discovered to be invalid. New ballistic weldments of 2519-T87 welded to itself were successfully qualified to the shock test in MIL-STD-1946.

AD UNCLASSIFIED  
UNLIMITED DISTRIBUTION

Key Words

Weldability  
Aluminum alloys  
Mechanical properties

U.S. Army Materials Technology Laboratory  
Watertown, Massachusetts 02172-0001  
WELDABILITY OF 2519-T87 ALUMINUM  
ALLOY - Jack H. Devletian, Sandra M.  
DeVincent, and Steven A. Gedeon

Technical Report MTL TR 88-47, December 1988, 28 pp-  
illus-tables, D/A Project 16162105AH84, AMCMS  
Code 612105.H84

Test results show that 2519-T87 is weldable to itself and to 5083-H131. A wide variety of filler metals, weld parameters, and post-weld heat treatments were studied to determine the effect on weld mechanical properties, hot crack susceptibility, microstructure, and ballistic integrity. Previously reported 2519-T87 weldment ballistic failures have been discovered to be invalid. New ballistic weldments of 2519-T87 welded to itself were successfully qualified to the shock test in MIL-STD-1946.

AD UNCLASSIFIED  
UNLIMITED DISTRIBUTION

Key Words

Weldability  
Aluminum alloys  
Mechanical properties